Charge counting statistics and weak localization in a quantum chain

G. C. Duarte-Filho,[1] F. A. G. Almeida,[1] S. Rodríguez-Pérez,[2] and A. M. S. Macêdo[3]

[1]*Departamento de Física, Universidade Federal de Sergipe 49100-000 São Cristóvão, Sergipe, Brazil*

[2]*Departamento de Física, Universidade Federal de São Carlos, São Paulo, Brazil*

[3]*Departamento de Física, Laboratório de Física Teórica e Computacional,Universidade Federal de Pernambuco 50670-901 Recife, Pernambuco, Brazil*

(Received 19 October 2012; revised manuscript received 7 January 2013; published 4 February 2013)

We study transport properties of a quantum chain formed by an array of chaotic quantum dots coupled to each other and to electron reservoirs via barriers of arbitrary transparencies. We introduce two exact representations of the generating function (GF) of charge counting statistics: a transfer matrix model for numerical simulations and a supersymmetric σ model for analytical calculations. Using the σ model, we calculate analytically the semiclassical term and the leading quantum correction (weak localization) of GF as a function of barriers' transparencies and the number of quantum dots. We observe that the density of transmission eigenvalues, obtained from the semiclassical term of the GF, exhibits a quantum transition, associated with the emergence of Fabry-Perot modes, in a region of the parameter space of barriers' transparencies that expands by increasing the number of quantum dots in the chain. Simple analytical expressions for the transition lines are derived, which may be used to tune the different regimes. We demonstrate that the presence of these Fabry-Perot (FP) modes plays a decisive role in controlling the ballistic-diffusive crossover in the quantum chain. We also find interesting nonmonotonic behaviors in the leading semiclassical terms and changes of sign in the weak-localization corrections of high-order charge transfer cumulants, as a function of the number of dots. Our results agree well with independent analytical calculations using a diagrammatic technique for integration over the unitary group and also with numerical simulations using the transfer matrix model.

DOI: 10.1103/PhysRevB.87.075404 PACS number(s): 73.23.−b, 73.21.La, 73.21.Hb, 05.45.Mt

I. INTRODUCTION

Nanoscale and microscale devices based on semiconductor heterostructures, such as quantum dots and quantum wires, provide natural laboratories in which to study quantum signatures of electron transport in the presence of complete or partial phase coherence.[1] The possibility one has to control the relevant parameters in such systems has had a great impact in the development of the theoretical approaches to quantum transport in artificial devices. More recently, much attention have been given to complex devices, such as quantum networks formed by arrays of quantum dots on GaAs, arranged in various geometries, such as chains[2–4] and honeycomb patterns.[5–7] The possibility of building artificial quantum simulators of complex many-body systems in this way is an exciting perspective that may come out from these efforts.[8,9]

The study of the process of transferring particles through quantum devices led to the concept of charge counting statistic (CCS),[10] a fermionic version of the photon counting statistics developed by Glauber in 1963.[11] The central concept of CCS is the probability, $P_n(T_{\rm ob})$, that n units of charge are transferred during an observation time $T_{\rm ob}$. The randomness on the quantum transmission process, and the Pauli principle, play an important role in the value of $P_n(T_{\rm ob})$. The CCS of a phase coherent conductor is fully characterized by a characteristic or cumulant generating function, $\Phi(\lambda)$, defined via the Fourier series $e^{\Phi(\lambda)} \equiv \sum_n P_n(T_{\rm ob})e^{{\rm in}\lambda}$. In Ref. 10, the cumulant generating function of a quantum device was calculated in terms of its transmission eigenvalues $\{\tau_i\}$, i.e., the eigenvalues of $tt^\dagger$, where t is the transmission matrix of the device. More recently, a powerful connection has been found between the CCS of a quantum point contact and the entanglement entropy,[12] which may allow a direct measurement of entanglement via current fluctuations. A particularly interesting result is the reconstruction of the full entanglement spectrum, i.e., the full set of eigenvalues of the reduced density matrix, via high-order CCS cumulants.[13] In Ref. 14, a unified approach based on fluctuation theorems was proposed to describe nonequilibrium properties, such as charge transfer statistics, of open quantum systems. A central concept in this approach is the notion of two-point projective measurements. It was shown that several known approaches to quantum transport can be recovered by taking particular cases of two-point measurements. For instance, a trajectory approach can be obtained from an interpretation of the quantum master equation in terms of continuous positive operator measurements for systems weakly coupled to reservoirs.[15] Another approach that can be recovered is the modified propagator technique defined via the Keldysh Green's function, which can be used to calculate $\Phi(\lambda)$ of an arbitrary quantum device. Semiclassical approaches to quantum scattering theory have also been used to obtain $\Phi(\lambda)$.[16] A different route to obtain the CCS generating function of a quantum device was put forward in Ref. 17 using the language of many-body physics. In this work, the microscopic description of the whole system, including the detectors, is treated in a quantum many-body language. The dynamics of the system is obtained via the projective technique of nonequilibrium statistical mechanics, combined with an extended-in-time measurement scheme. The main result obtained from this approach is a general formula expressing $\Phi(\lambda)$ in terms of the many-body Green's function of the device.

An important universal transport regime appears when the quantum device is a network of ballistic chaotic cavities coupled to each other via potential barriers. In this case, a random matrix approach[18] applies, and it predicts that the

transmission eigenvalues of the conductor become strongly correlated random variables. This means that the generating function $\Phi(\lambda)$ fluctuates, and can no longer be considered a complete characterization of the stochastic process associated with charge transfer. In the semiclassical regime, characterized by a large number of open transmission channels, we may neglect such fluctuations and calculate the average generating function $S(\lambda) = \langle \Phi(\lambda) \rangle$ using a quantum circuit theory (QCT).[1] The main advantage of QCT is the fact that one can calculate $S(\lambda)$ directly as a function of the system's control parameters without having to obtain first the joint distribution of transmission eigenvalues. In Ref. 19, it was shown how to extend QCT to obtain weak localization (WL) corrections and universal fluctuations of transport observables.

Experimental realizations of quantum networks with the topology of a chain show an interesting ballistic-diffusive crossover,[2,3] evidence of localization effects.[4] In Ref. 3, experimental results for the Fano factor, defined as the ratio between the second and the first charge transfer cumulant, as a function of the number of dots in the chain were compared with theoretical results obtained from the Boltzmann-Langevin semiclassical formalism.[20] A study of this crossover using the first three charge transfer cumulants, obtained from QCT, was presented in Ref. 21. Continuous advances in measurement techniques of high-order charge transfer cumulants[22] suggest that experimental data, for at least the first three charge transfer cumulants, may soon be available for several types of quantum networks. The recently found connection between high-order cumulants and the full entanglement spectrum[13] provides another motivation for the development of effective methods to calculate and analyze these cumulants for arbitrary quantum networks.

In this paper, we present a detailed study of charge transfer cumulants, including weak-localization (WL) corrections, for a chain of quantum dots coupled to each other, and to electron reservoirs, via barriers of arbitrary transparencies. Our analytical results provide an essentially complete description of the ballistic-diffusive crossover, by showing explicitly the dependence on the number of dots in the chain and on all barriers' transparencies. Furthermore, we observe that the density of transmission eigenvalues, obtained from the dominant semiclassical contribution to $S(\lambda)$, exhibits a quantum transition, associated with the emergence of Fabry-Perot modes, in a region of the parameter space of barriers' transparencies that expands by increasing the number of quantum dots in the chain. We demonstrate that the presence of these Fabry-Perot modes plays a decisive role in controlling the ballistic-diffusive crossover in the quantum chain. Crossovers from pure symmetry ensembles are also accounted for by calculating $S(\lambda)$ in terms of the rates for spin-orbit scattering and magnetic-field decoherence. Our results agree well with those obtained from a diagrammatic technique for integration over the unitary group[23] and with numerical simulations using random unitary matrices.[24]

This paper in organized as follows. In Sec. II, we discuss a model for the coupling between adjacent quantum dots and introduce a mathematical description of charge transfer statistics in a chain of quantum dots by means of a nonlinear σ model. In Sec. III, we derive the equations of quantum circuit theory for a quantum chain. These equations are used to calculate the dominant semiclassical contributions to the first four charge transfer cumulants of two types of quantum chains: (i) a homogenous array, described as a chain where all barriers connecting adjacent dots have the same transparency, and (ii) a heterogenous array, where there are one or several connectors with transparencies that differ from those of the rest of the chain. In the latter case, we also study the density of transmission eigenvalues of the chain. We observe the emergence of Fabry-Perot modes in a certain region in parameter space, and we describe how it depends on the number of quantum dots in the chain. In Sec. IV, we apply quantum circuit theory to the calculation of WL corrections. We derive a generating function for the WL corrections of charge transfer cumulants of a homogenous chain, and use it to calculate explicit expressions for WL corrections of the first three cumulants as a function of the number of dots and the transparencies of the barriers. The WL corrections of high-order cumulants agree well with numerical simulations based on random unitary matrices. We also present an analytical expression for the WL correction of the conductance of the chain including crossover parameters, which generalizes several recent results of the literature. A summary and conclusions are presented in Sec. VI.

II. STATISTICS OF CHARGE TRANSFER THROUGH A QUANTUM CHAIN

In this section we introduce a model that describes the statistics of charge transfer through an array of quantum dots, coupled to each other and to electron reservoirs via potential barriers. The reservoirs are in thermodynamical equilibrium characterized by a Fermi-Dirac distribution $f_{\mathrm{L(R)}}(E)$. The potential drop across the system is given by $eV = \mu_L - \mu_R$, where μ_L (μ_R) is the chemical potential in the left (right) reservoir and e is the electron charge. In Fig. 1 we give a pictorial representation of our system.

We now discuss a mathematical representation of the generating function for the counting statistics of charge transfer through the chain. Following Ref. 25, we start from the Levitov-Lesovik expression for the generating function[10] of charge transfer through a generic device characterized by its transmission matrix $\mathbf{t}(E)$:

$$\Phi(\lambda) = -\frac{T_{\mathrm{ob}}}{h}\int_{-\infty}^{\infty} dE\, \mathrm{Tr}\ln[\mathbf{1} + J_\lambda(E)\mathbf{t}(E)\mathbf{t}^\dagger(E)], \quad (1)$$

where T_{ob} is the observation time, λ is the counting parameter, $J_\lambda(E) = (e^{i\lambda} - 1) f_1(E)[1 - f_2(E)] + (e^{-i\lambda} - 1) f_2(E)[1 - f_1(E)]$, and $f_j(E)$ is the Fermi-Dirac distribution function in the jth reservoir. We assume universal chaotic dynamics inside the dots, which implies that $\mathbf{t}(E)$ can be described by a random matrix, and that we may neglect its energy dependence. Consequently, $\Phi(\lambda)$ is a random function and an average over its realizations has to be performed. There is an exact procedure to do this, known as the supersymmetry technique.[26] One of the advantages of this approach is the possibility of accessing both the perturbative and nonperturbative physical regimes, which correspond to large and small numbers of open scattering channels respectively.

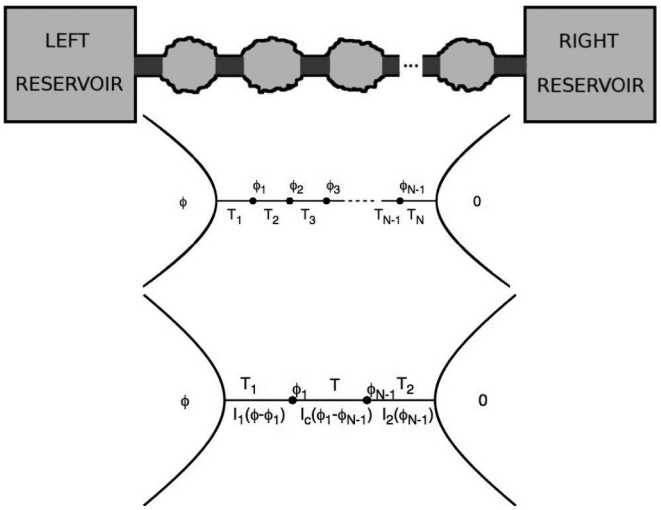

FIG. 1. At the top, we show a pictorial representation of a linear array of quantum dots connected to each other via nonideal contacts. The dots at the boundaries are connected to a left (L) and a right (R) electron reservoir, characterized by Fermi distribution functions with chemical potentials given by μ_L and μ_R respectively. In the middle, we have a circuit representation of the array, in which every dot is labeled by a member of a set of auxiliary variables $\{\phi_i\}$. The variable ϕ in the left reservoir plays the role of a pseudopotential in the language of quantum circuit theory. Each connector coupling adjacent dots, or an outer dot to a reservoir, is characterized by a transmission coefficient T_i and a number N_i of equivalent propagation channels. At the bottom, we show an effective two-dot representation of a chain in which all internal connectors have transmission coefficient equal to T.

We proceed by considering the following average ratio of determinants[27]

$$\Psi(\phi_0,\theta_0)=\left\langle \det\left(\frac{1-\sin^2(\phi_0/2)\mathbf{t}\mathbf{t}^\dagger}{1-\sinh^2(\theta_0/2)\mathbf{t}\mathbf{t}^\dagger}\right)\right\rangle, \tag{2}$$

where ϕ_0 and θ_0 are auxiliary variables. The connection between $\Psi(\phi_0,\theta_0)$ and the ensemble average of $\Phi(\lambda)$ is obtained via the auxiliary function

$$\begin{aligned} q(\lambda) &= i\frac{\partial\langle\Phi(\lambda)\rangle}{\partial\lambda} \\ &= -i\frac{T_{\rm ob}}{h}\int_{-\infty}^{\infty} dE\,\frac{\partial J_\lambda(E)}{\partial\lambda}\,\frac{K[\sinh^{-1}\sqrt{J_\lambda(E)}]}{\sqrt{J_\lambda(E)[1+J_\lambda(E)]}}, \end{aligned}$$

where $K(x)$ is given by

$$\begin{aligned} K(x) &= \frac{1}{2}\left\langle \mathrm{Tr}\left(\frac{\sinh(2x)\mathbf{t}\mathbf{t}^\dagger}{1+\sinh^2(x)\mathbf{t}\mathbf{t}^\dagger}\right)\right\rangle \\ &= -i\frac{\partial\Psi(\phi_0,\theta_0)}{\partial\phi_0}\bigg|_{\phi_0=-2ix=i\theta_0}. \end{aligned} \tag{3}$$

The ensemble average shown in Eqs. (2) and (3) can be calculated numerically using a random scattering matrix model. The numerical procedure requires a generator of random unitary matrices from the circular Wigner-Dyson ensemble.[28] The universal chaotic dynamics inside each dot can be modeled by sampling a scattering matrix, $\mathbf{S}_j$, from this generator. Due to the multiplicative rule of the transfer matrix of a chain in terms of the transfer matrices of the dots and the connectors, it is convenient to convert the scattering matrix of the dot, $\mathbf{S}_j$, into a transfer matrix, $\mathbf{M}_j$. The transfer matrix of the jth connector can be written as[24,29]

$$\mathcal{M}_j=\begin{pmatrix} t_j^{-1}\mathbf{1} & r_j t_j^{-1}\mathbf{1} \\ -r_j t_j^{-1}\mathbf{1} & t_j^{-1}\mathbf{1}\end{pmatrix}, \quad j=1,\ldots,N, \tag{4}$$

where $\mathbf{1}$ is the $N_c\times N_c$ identity matrix, N_c is the number of open channels in the connector, and $r_j=i\sqrt{1-T_j}$ and $t_j=\sqrt{T_j}$ are the reflection and transmission amplitudes of the connector respectively. The transfer matrix of the whole system is obtained from the following matrix product:[24,29]

$$\mathbf{M}=\mathcal{M}_1\mathbf{M}_1\mathcal{M}_2\mathbf{M}_2\mathcal{M}_3\cdots\mathbf{M}_{N-1}\mathcal{M}_N. \tag{5}$$

Equation (5) is the main formula for the implementation of our numerical procedure.

In analytical calculations, we may proceed by using the supersymmetry technique[26] to represent $\Psi(\phi_0,\theta_0)$ as a propagator of a supersymmetric nonlinear σ model,

$$\Psi(\phi_0,\theta_0)=\int_{\hat{Q}_j^2=1}\prod_{j=1}^{N-1} d\hat{Q}_j e^{S(\{\hat{Q}\})}, \tag{6}$$

in which $\hat{Q}_j$ are supermatrices associated with each dot in the chain. The σ-model action is given by

$$S(\{\hat{Q}\})=\sum_{j=0}^{N-1}\mathcal{S}_j(\hat{Q}_j,\hat{Q}_{j+1}), \tag{7}$$

where

$$\mathcal{S}_j(\hat{Q}_j,\hat{Q}_{j+1})=-\frac{N_c}{4}\mathrm{Str}\ln\left(1-\frac{T_{j+1}}{4}(\hat{Q}_j-\hat{Q}_{j+1})^2\right), \tag{8}$$

in which N_c is the number of open scattering channels in the chain and T_{j+1} is the transmission coefficient of the $(j+1)$th connector. We defined the indices such that the supermatrix $\hat{Q}_0\equiv\hat{Q}_\phi$ describes the left reservoir, while $\hat{Q}_N$ describes the right one. Although we do not provide here a formal proof of the equivalence between the random transfer matrix representation, Eq. (5), and the supersymmetric σ-model representation, Eq. (6), detailed comparisons between these representations will be made via explicit calculations of the first four charge transfer cumulants.

An alternative formulation of charge counting statistics using the nonequilibrium Keldysh Green's function technique was put forward in Refs. 30 and 31. In this formalism, the counting field is introduced via a gauge transformation and the effective action coincides with Eq. (7), after appropriate redefinitions of the trace operation and the $\hat{Q}_j$ matrices, which acquire a Keldysh structure. The main result of the Keldysh approach is the derivation, via the extremum of the action, of a matrix version of quantum circuit theory of charge counting statistics at finite temperature.[30] In the above supermatrix formalism, an equivalent quantum circuit theory emerges from the evaluation of Eq. (6) using the saddle-point approximation. In both approaches the resulting equations are scalar for a two-terminal setup. The main advantage of the supersymmetry approach, however, is the possibility to perform nonperturbative calculations, which are essential,

for instance, to understand the transition from the metallic to the insulating regimes in the network[32,33] A detailed comparison between the Keldysh and supersymmetry approaches was presented in Ref. 25.

III. QUANTUM CIRCUIT THEORY

In this section we describe the supersymmetric version of quantum circuit theory (QCT) relevant to the statistics of charge transfer through a quantum chain. We show how it emerges from the saddle-point approximation of Eq. (6) and we use it to calculate charge transfer cumulants of several types of chains as a function of the number of connectors in the circuit. We also calculate the average density of transmission eigenvalues of a heterogeneous chain.

We start by connecting the average dimensionless generating function, $S(\lambda) \equiv h\langle\Phi(\lambda)\rangle/(eVT_{\rm ob})$, to the average density of transmission eigenvalues, $\rho(\tau) = \sum_n \langle\delta(\tau-\tau_n)\rangle$, at zero temperature and low voltages. With the condition of universal chaotic dynamics inside the dots we may neglect the energy dependence of the transmission eigenvalues; we thus find

$$S(\lambda) = \int_0^1 d\tau\, \rho(\tau) \ln[1+\tau(e^{i\lambda}-1)]. \tag{9}$$

In the semiclassical regime, the number of open scattering channels is large and $\rho(\tau)$ becomes a smooth function. From a technical point of view it is convenient to introduce a new counting parameter ε given by

$$\varepsilon^2 = 1 - e^{i\lambda}, \tag{10}$$

and to define the following auxiliary function

$$g(\varepsilon) = -i\frac{\partial S(\lambda)}{\partial\lambda}\bigg|_{e^{i\lambda}=1-\varepsilon^2} = \int_0^1 d\tau\, \rho(\tau)\frac{(1-\varepsilon^2)\tau}{1-\varepsilon^2\tau}, \tag{11}$$

from which the charge transfer cumulants can be obtained through the formula

$$q_{l+1} = \left(\frac{\varepsilon^2-1}{2\varepsilon}\frac{d}{d\,\varepsilon}\right)^l g(\varepsilon)\bigg|_{\varepsilon=0}, \quad l = 0,1,\ldots. \tag{12}$$

It is also convenient to introduce the change of variables $\tau = \mathrm{sech}^2 x$, and to define a new average density $\nu(x)$, which can be obtained from $g(\varepsilon)$ through

$$\nu(x) = \frac{2}{\pi}\mathrm{Im}\left\{\frac{i\varepsilon}{\sqrt{1-\varepsilon^2}}g(\varepsilon)\bigg|_{\varepsilon=\cosh x}\right\}. \tag{13}$$

The density $\nu(x)$ is directly related to $\rho(\tau)$ via the transformation formula

$$\rho(\tau) = \frac{\nu[\cosh^{-1}(1/\sqrt{\tau})]}{2\tau\sqrt{1-\tau}}. \tag{14}$$

We proceed by introducing a function $I(\phi)$ which, in the saddle-point approximation, plays the role of a conserving pseudocurrent. In the nonperturbative sector it is connected to the propagator of the nonlinear σ model, $\Psi(\phi_0,\theta_0)$, via[25]

$$I(\phi) = -2\frac{\partial\Psi(\phi_0,\theta_0)}{\partial\phi_0}\bigg|_{\phi_0=\phi=i\theta_0}. \tag{15}$$

The relation between $I(\phi)$ and $g(\varepsilon)$ is given by

$$g(\varepsilon) = \frac{\sqrt{1-\varepsilon^2}}{2\varepsilon}I(\phi)\bigg|_{\sin(\phi/2)=\varepsilon}. \tag{16}$$

In the semiclassical regime characterized by a large number of propagating modes, $N_c \gg 1$, we may evaluate $\Psi(\phi_0,\theta_0)$ using the saddle-point approximation. The saddle-point equations are obtained from the extremum of $S(\{\hat{Q}\})$ with respect to Q_j, for $j = 1,\ldots,N-1$, under the constraint $\hat{Q}_j^2 = 1$. The resulting equations can be interpreted as a conservation law for a supermatrix current. One can greatly simplify these equations by the use of the following parametrization for the matrices $\hat{Q}_j$:

$$\hat{Q}_j = \begin{pmatrix} 0 & e^{-i\hat{\Phi}_j} \\ e^{i\hat{\Phi}_j} & 0 \end{pmatrix}, \tag{17}$$

where $\hat{\Phi}_j = \mathrm{diag}(i\theta_j, i\theta_j, \phi_j, \phi_j)$, for $j = 0,\ldots,N$, with the boundary conditions $\theta_0 = -i\phi$, $\theta_N = 0$, $\phi_0 = \phi$, and $\phi_N = 0$. With this parametrization the action reads

$$\mathcal{S}(\{\hat{Q}\}) = N_c\sum_{j=0}^{N-1}\ln\left(1 - T_{j+1}\sin^2(\Delta\phi_{j+1}/2)\right) - N_c\sum_{j=0}^{N-1}\ln\left(1 - T_{j+1}\sinh^2(\Delta\theta_{j+1}/2)\right),$$

where $\Delta\phi_{j+1} = \phi_j - \phi_{j+1}$ and $\Delta\theta_{j+1} = \theta_j - \theta_{j+1}$. The saddle-point equations are obtained from

$$\frac{\partial\mathcal{S}}{\partial\phi_j} = 0 = \frac{\partial\mathcal{S}}{\partial\theta_j}, \quad j = 1,\ldots,N-1, \tag{18}$$

and can be used to calculate $\Psi(\phi_0,\theta_0)$ with logarithmic accuracy. After using Eq. (15), we obtain the following conservation laws for a scalar pseudocurrent:

$$I(\phi) = I_1(\phi-\phi_1) = \cdots = I_j(\phi_{j-1}-\phi_j) = \cdots = I_N(\phi_{N-1}) \tag{19}$$

where

$$I_j(\Delta\phi_j) = \frac{N_c T_j\sin(\Delta\phi_j)}{1 - T_j\sin^2(\Delta\phi_j/2)}, \quad j = 1,2,\ldots,N. \tag{20}$$

We remark that Eqs. (19) and (20) can also be obtained via the Keldysh approach.[30]

The problem is thus reduced to the determination of the pseudopotentials ϕ_j at all nodes of the circuit. We shall apply this procedure to two interesting cases: a homogenous linear array and a heterogeneous chain.

A. Homogeneous chain

The homogeneous chain is obtained by setting $T_j = T$ at all connectors. The physical solution of Eq. (19) can be obtained from the set of equations $\sin(\Delta\phi_j) = \sin(\Delta\phi_{j-1})$, for $j = 1,\ldots,N$, with the boundary conditions, $\phi_0 = \phi$, and $\phi_N = 0$. We obtain $\phi_j = (N-j)\phi/N$, which gives the following expression for the pseudocurrent:

$$I(\phi) = \frac{N_c T\sin(\phi/N)}{1 - T\sin^2(\phi/2N)}. \tag{21}$$

Substituting Eq. (21) into Eq. (16), and expanding the result in powers of ε, we obtain

$$\frac{g(\varepsilon)}{N_c} = \frac{T}{N} - \frac{T}{3}\frac{(N^2+2-3T)}{N^3}\varepsilon^2 + \frac{T}{15}\frac{[2(1-N^4)-15(1-T)T]}{N^5}\varepsilon^4 + \frac{T}{315N^7}[-24N^6+(14-21T)N^4+(14-105(1-T)T)N^2+315T^3-420T^2+126T-4]\varepsilon^6+\mathcal{O}(\varepsilon^8), \quad (22)$$

Using Eq. (12) we can calculate the ratios of the second (shot noise), third (skewness), and fourth (curtosis) cumulants to the conductance of the system. We find

$$F \equiv \frac{q_2}{q_1} = \frac{1}{3} + \frac{1}{3}\frac{2-3T}{N^2}, \quad (23)$$

$$S \equiv \frac{q_3}{q_1} = \frac{1}{15} + \frac{1}{3}\frac{2-3T}{N^2} + \frac{2}{15}\frac{2-15(1-T)T}{N^4}, \quad (24)$$

$$Q \equiv \frac{q_4}{q_1} = -\frac{1}{105} + \frac{1}{5}\frac{2-3T}{N^2} - \frac{4}{5}\frac{15(1-T)T-2}{N^4} - \frac{2}{105}\frac{315T^3-420T^2+126T-4}{N^6}. \quad (25)$$

The expressions for the Fano factor (F) and the skewness-conductance ratio (S) agree with those obtained in Ref. 21 using a matrix version of quantum circuit theory.

In Fig. 2 we show the behaviors of F, S, and Q as a function of the number of connectors N for several values of T. The behaviors of F and S reproduce those obtained in Ref. 3 using a Boltzmann-Langevin approach. In both graphs we can see an increasing monotonic behavior for $T = 0.7$ (green lines), and $T = 1$ (red lines) approaching

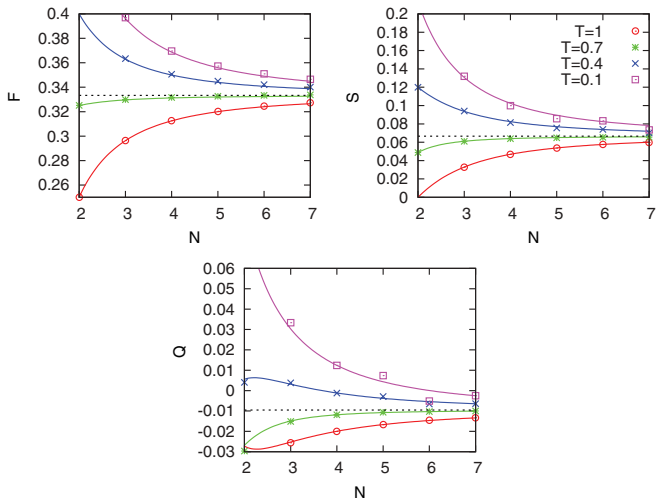

FIG. 2. (Color online) Behavior of three transport observables as a function of the number of connectors for several barrier transparencies. The analytical results for the Fano factor F (top left), the ratio of the skewness to the conductance S (top right), and the ratio of the curtosis to the conductance Q (bottom) are plotted with red lines for $T = 1$, green lines for $T = 0.7$, blue lines for $T = 0.4$, and magenta ones for $T = 0.1$. The horizontal dashed lines show the values of F, S, and Q for a quantum wire: 1/3, 1/15, and $-1/105$ respectively. The numerical data are represented by a different symbol for each transparency value.

the expected values in the quantum wire limit, $F_{\text{wire}} = 1/3$ and $S_{\text{wire}} = 1/15$ respectively, as we increase the number of connectors. It is interesting to observe that there exists a value close to $T = 0.7$ at which the observables tend faster to the quantum wire values, as can be seen in Fig. 2, where the quantum wire limit is reached already for a small number of connectors, $N \approx 5$. This feature is consistent with shot-noise measurements by Oberholzer *et al.*[2,3] Furthermore, note that the curtosis-conductance ratio (Q) displays a nonmonotonic behavior for intermediate values of T and tends to the quantum wire limit, $-1/105$, for large N. It is also interesting to notice that, at $T = 2/3$, the first correction term $\mathcal{O}(N^{-2})$ due the discreteness of the chain vanishes for F, S, and Q. Remarkably, the Fano factor of the chain becomes independent of N at $T = 2/3$.

We stress that our results are in complete agreement with the numerical simulations using the transfer matrix model, which are presented in Fig. 2 with symbols. The numerical procedure consists of extracting the transmission eigenvalues from the random transfer matrix of the chain, **M** [see Eq. (5)], and the transport observables (e.g., conductance, shot noise power, etc.) are calculated for each realization. We generated 10^5 realizations of the matrix ensemble, which proved to be sufficiently large to estimate the averages of the observables. The semiclassical limit was reached by the following procedure: we obtained results for $N_c = 20, 21, \ldots, 50$, and then numerically extrapolated to $N_c \to \infty$.

In the next subsection we describe how a nonhomogeneity, due to a pair of barriers with transparencies different from all the others in the chain, uncovers a key ingredient in the ballistic-diffusive crossover.

B. Heterogenous Chain

In this section we apply quantum circuit theory to the heterogeneous setup described in Fig. 1. We focus our attention on a circuit with only four adjustable parameters, three of which are barrier's transparencies shown in Fig. 1. We distinguish between the connectors joining adjacent dots, with transparency T, and barriers which connect the external dots in the chain to the reservoirs, with transparencies T_1 and T_2. The remaining parameter is the number of quantum dots in the chain. A key simplification in this configuration arises from the translational symmetry of the pseudopotential drops between adjacent dots in the array (similar to the homogenous case discussed above), which allows, as we show below, the reduction of the initial problem of $N - 1$ coupled quantum dots into a problem of two coupled quantum dots (see Fig. 1).

Applying quantum circuit theory to this heterogeneous chain, we obtain the following equations for the pseudo-current

through the connectors:

$$I_1(\phi-\phi_1)=\frac{N_cT_1\sin(\phi-\phi_1)}{1-T_1\sin^2[(\phi-\phi_1)/2]},$$

due to the "potential drop" through the barrier T_1,

$$I_{j,j+1}(\phi_j-\phi_{j+1})=\frac{N_cT\sin(\phi_j-\phi_{j+1})}{1-T\sin^2[(\phi_j-\phi_{j+1})/2]},$$

with $j=1,\ldots,N-1$, which describes the pseudocurrent through the internal connectors, and finally

$$I_2(\phi_{N-1})=\frac{N_cT_2\sin(\phi_{N-1})}{1-T_2\sin^2(\phi_{N-1}/2)},$$

due to the "potential drop" through the barrier T_2.

The pseudocurrent conservation law in the circuit reads

$$I_1(\phi-\phi_1)=I_{j,j+1}(\phi_j-\phi_{j+1})=I_2(\phi_{N-1}). \tag{26}$$

Taking into account the translational symmetry inside the chain, we conclude that the potential drop in any internal connector satisfies the equations

$$\sin(\phi_j-\phi_{j+1})=\sin\left(\frac{\phi_1-\phi_{N-1}}{N-2}\right),\quad j=1,2,\ldots,N-2,$$

which means that we can rewrite the conservation law, Eq. (26), in the reduced form

$$I_1(\phi-\phi_1)=I_c(\phi_1-\phi_{N-1})=I_2(\phi_{N-1}), \tag{27}$$

in which we defined the effective pseudocurrent

$$I_c(\phi_1-\phi_{N-1})=\frac{N_cT\sin[(\phi_1-\phi_{N-1})/(N-2)]}{1-T\sin^2[(\phi_1-\phi_{N-1})/(2N-4)]}. \tag{28}$$

related to the total pseudopotential drop in the internal chain. One can see that the problem of $N-1$ quantum dots was reduced, through a kind of decimation procedure, into an effective problem of two quantum dots coupled to each other via a renormalized connector. The pseudopotentials ϕ_1 and ϕ_{N-1} are found by numerically solving the effective pseudocurrent conservation laws, Eq. (27). We use this numerical procedure to calculate the density, $\nu(x=0)$, inside the chain. This quantity was introduced in Ref. 34 for a single quantum dot, where it was shown to behave like an "order parameter" as a function of the barriers' transparencies. The related quantum transition indicates the appearance of Fabry-Perot modes associated with ideal transmission eigenvalues ($\tau=1$ or $x=0$). Signatures of a similar quantum transition have been found in the tails of the transmitted charge distribution of a single quantum dot with nonideal contacts[35] and in the charge-transfer statistics of a quantum dot connected to a normal metal and to a superconducting reservoir via two potential barriers.[36]

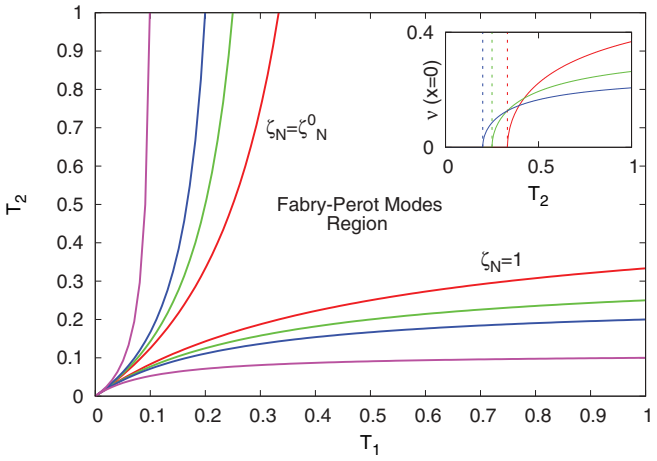

FIG. 3. (Color online) $T_1\times T_2$ diagram for $T=1$, and $N=3$ (red lines), $N=4$ (green), $N=5$ (blue), and $N=10$ (magenta). The regions inside the curves $\zeta_N=1$ and $\zeta_N=\zeta_N^0$ with the same color correspond to the regime where the system sustains Fabry-Perot modes, i.e., $\nu(x=0)>0$. The inset shows the behavior of the "order parameter" $\nu(x=0)$ for $T_1=T=1$ for $N=3$, $N=4$, and $N=5$ connectors as a function of T_2. The vertical dashed lines indicates the special values of T_2, for each fixed number of connectors, where we observe the emergence of Fabry-Perot modes.

In Fig. 3, we show the transition lines [points where $\nu(x=0)$ vanishes] in the T_1T_2 plane, for different numbers of connectors. In the inset we show the behavior of $\nu(x=0)$ as a function of N and T_2 with $T_1=1=T$. We observe that for $N=3$, i.e., a circuit with two dots, $\nu(x=0)$ vanishes for $T_2\leqslant 1/3$, and is nonzero otherwise. We remark that in the $N=2$ case, where there is a single dot,[34] the transition point for $T_1=1$ is $T_2^c(N=2)=1/2$. In the case of $N-1$ dots in the chain and $T_1=1=T$, we obtain $T_2^c(N)=1/N$. We may generalize this result to the case where T_1, T_2 and T are arbitrary, through the following auxiliary variables

$$\zeta_N=\frac{T_2}{T_1}\left(1+(N-2+T)\frac{T_1}{T}\right) \tag{29}$$

and

$$\zeta_N^0=\frac{1+(N-2+T)\frac{T_1}{T}}{1-(N-2+T)\frac{T_1}{T}}. \tag{30}$$

In Fig. 3 (main plot), we show the transition lines defined by $\zeta_N=1$ and $\zeta_N=\zeta_N^0$ in the T_1T_2-plane for $T=1$. The region between the curves gives the support of $\nu(x=0)$ and corresponds to the parameter values at which the system sustains a finite density of Fabry-Perot modes, thus generalizing the single-dot results of Ref. 34.

Let us now turn to the charge transfer cumulants of the heterogenous chain. For the sake of simplicity, we set $T=T_1$, so that we are left with only two free parameters, T_1 and T_2. In this case, the equivalent circuit contains only one dot. The pseudocurrent in the connectors are given by

$$I_1(\phi-\phi_1)=\frac{2N_cT_1\tan\left(\frac{\phi-\phi_1}{2(N-1)}\right)}{1+(1-T_1)\tan^2\left(\frac{\phi-\phi_1}{2(N-1)}\right)} \tag{31}$$

and

$$I_2(\phi_1) = \frac{2N_c T_2 \tan(\phi_1/2)}{1 + (1 - T_2)\tan^2(\phi_1/2)}. \tag{32}$$

From the pseudo-current conservation law, $I(\phi) = I_1(\phi - \phi_1) = I_2(\phi_1)$, we find ϕ_1 and thus $I(\phi)$, which we then insert into Eq. (16) to obtain $g(\varepsilon)$. Expanding $g(\varepsilon)$ in powers of ε, we calculate the Fano factor F and the skewness-conductance ratio S. The results are

$$F = \frac{1}{3}\frac{(nT_2 + 3T_1)n^2T_2^2 + \left[(2 - 3T_1)T_2^2 + 3T_1^2\right]nT_2 + 3(1 - T_2)T_1^3}{(T_1 + nT_2)^3} \tag{33}$$

$$\begin{aligned} S = \frac{1}{15(T_1 + nT_2)^6}\big\{&(nT_2 + 6T_1)n^5T_2^5 + 5\left[(2 - 3T_1)T_2^2 + 3T_1^2\right]n^4T_2^4 + 15\left[(2 - 3T_1)T_2^2 + (2 - T_2)T_1^2\right]n^3T_1T_2^3 \\ &+ \left[2\left(2 - 15(1 - T_1)T_2^4\right) + 15(2 - 3T_1)T_1^2T_2^2 + 45(1 - T_2)T_1^4\right]n^2T_2^2 + \left[6\left(-6 + 15T_1 - 10T_1^2\right)T_2^3\right. \\ &\left. + 60(2 - 3T_1)T_1^2T_2^2 + 15\left(6 - 9T_1 - 4T_1^2\right)T_1^2T_2 + 45T_1^4\right]nT_1T_2^2 + 15(1 - (3 - 2T_2)T_2)T_1^6\big\}, \end{aligned} \tag{34}$$

where $n = N - 1$ is the number of quantum dots in the chain. In the limit of large N these ratios behave as follows: $F = 1/3 + f(T_1,T_2)N^{-2} + \mathcal{O}(N^{-3})$ and $S = 1/15 + f(T_1,T_2)N^{-2} + \mathcal{O}(N^{-3})$, where $f(T_1,T_2) = 2/3 - T_1$. We remark that $1/3$ and $1/15$ are the values of these observables in the quantum wire limit.

In Fig. 4 we show the behavior of F and S for several values of N as a function of T_1 with fixed $T_2 = 0.1$ (left side of Fig. 4), and also the other way around, as a function of T_2 with fixed $T_1 = 0.1$ (right side). The dashed lines represent the values of F and S in the diffusive quantum wire limit, which are $1/3$ and $1/15$ respectively. As shown in Ref. 37 these values can be easily derived from the density of transmission eigenvalues of a diffusive quasi-one-dimensional conductor

$$\rho_D(\tau) = \frac{g}{2}\frac{1}{\tau\sqrt{1 - \tau}}, \tag{35}$$

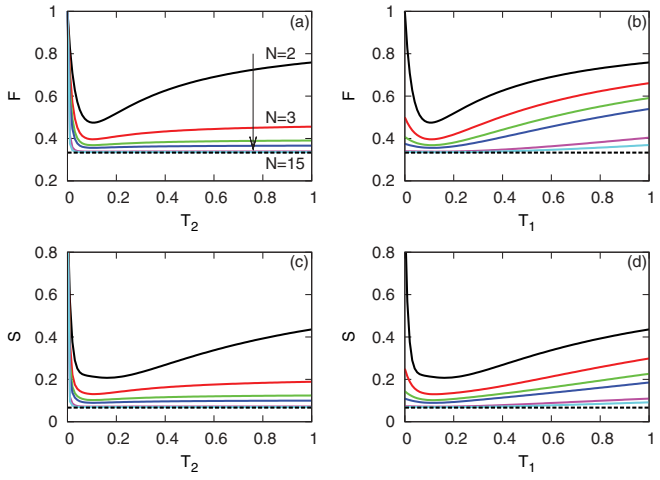

FIG. 4. (Color online) The behavior of the Fano factor, panels (a) and (b), and skewness-conductance ratio, panels (c) and (d), as a function of $T_2(T_1)$ with $T_1(T_2)$ fixed at the value 0.1, and $N = 2$ (black line), $N = 3$ (red), $N = 4$ (green), $N = 5$ (blue), $N = 11$ (magenta), and $N = 15$ (light blue). The vertical arrow in panel (a) indicates where the variable N increases. We observe a minimum in each curve indicating an attraction towards the diffusive limit caused by the presence of Fabry-Perot modes. The horizontal dotted lines show the expected values of F and S in the diffusive limit.

where g is the dimensionless conductance of the system. For instance, the Fano factor reads

$$F = \frac{\int_0^1 d\tau\, \rho_D(\tau)\tau(1 - \tau)}{\int_0^1 d\tau\, \rho_D(\tau)\tau} = \frac{1}{3}. \tag{36}$$

Note that the bimodal structure of $\rho_D(\tau)$ with an accumulation around the Fabry-Perot singularity at $\tau = 1$ is the central mechanism for the universal shot-noise reduction in this regime. In order to make contact with our results, note that from the transformation formula (14) we obtain $\nu_D(0) = g$, which indicates, since $g \gg 1$, that a diffusive conductor has a very large density of FP modes. By contrast, there are no FP modes in the insulating regime. From Fig. 4, we see that for $T_1 < 2/3$ both F and S exhibit nonmonotonic behavior as a function of the barriers' transparencies. We observe, in particular, a minimum in each curve indicating an attraction towards the diffusive limit caused by an increase in the density of the Fabry-Perot modes. We conclude that the introduction of an inhomogeneity in an array of quantum dots, via barriers of tunable transparencies, can change the density of FP modes and thus lead to some control over the charge transfer mechanism. This procedure may be used to delay or even suppress the emergence of the universal diffusive behavior.

In the next section we discuss the weak localization corrections for the charge transfer cumulants of a chain of quantum dots.

IV. WEAK LOCALIZATION

Campagnano and Nazarov[19] developed an interesting method to calculate the weak localization corrections of the charge transfer cumulants, which builds on quantum circuit theory and can be applied to quantum networks. The method provides a way to obtain the weak localization corrections directly from an expansion of the semiclassical action up to second order and the computation of eigenvalues of a finite element version of the Cooper propagator. The extension of this method to the supersymmetry action used here is straightforward and thus we shall concentrate our discussion on how to use the Cooper propagator eigenvalues, which we obtain from our model, to calculate the weak localization corrections of the charge transfer cumulants of the quantum chain.

Let $M_j^{\pm}(\phi)$ denote the eigenvalues of the finite element version of the Cooper propagator. The weak-localization correction to the pseudocurrent is given by[19]

$$I^{\rm wl}(\phi) = -2\frac{\partial}{\partial\phi}S^{\rm wl}(\phi), \tag{37}$$

where

$$S^{\rm wl}(\phi) = \frac{2-\beta}{2\beta}\sum_{j=1}^{N-1}\ln\left(\frac{M_j^+(\phi)}{M_j^-(\phi)}\right), \tag{38}$$

and β is Dyson's symmetry index. We must set $\beta = 1$ for systems with time-reversal (TR) symmetry and spin-rotation (SR) invariance, $\beta = 2$ for systems with broken TR, and $\beta = 4$ for systems with broken SR in the presence of TR symmetry.

Defining the auxiliary function

$$g^{\rm wl}(\varepsilon) = \frac{\sqrt{1-\varepsilon^2}}{2\varepsilon}I^{\rm wl}(\phi)\Big|_{\sin\phi/2=\varepsilon}, \tag{39}$$

the weak localization correction of the charge transfer cumulants can be obtained from the simple formula

$$q_{l+1}^{\rm wl} = \left(\frac{\varepsilon^2-1}{2\varepsilon}\frac{d}{d\varepsilon}\right)^l g^{\rm wl}(\varepsilon)\Big|_{\varepsilon=0}. \tag{40}$$

In the next subsections, we apply this procedure to obtain weak localization corrections to the first three charge transfer cumulant of some quantum chains.

A. Single dot

For the sake of comparison with previous works, we consider first the case $N = 2$, where the "chain" has only one quantum dot connected to reservoirs via barriers of arbitrary transparencies. The WL correction to the first two charge transfer cumulants was already calculated with the same technique in Ref. 38, where it was found to agree with independent diagrammatic technique for integration over the unitary group. Here we extend this result to include the WL correction to the third cumulant. The Cooper propagator eigenvalues for the single dot are obtained by applying the method of Ref. 19 to our σ-model action. We find

$$M^{\sigma}(\phi) = 2\sum_{j=1}^{2}N_jZ_j[\cos(\phi_{j-1}) + (\delta_{\sigma,+})2Z_j\sin^2(\phi_{j-1})], \tag{41}$$

where

$$Z_j = \frac{T_j}{4-4T_j\sin^2(\Delta\phi_j/2)}, \tag{42}$$

with $\Delta\phi_j = \phi_{j-1} - \phi_j$, $\phi_0 = \phi$, $\phi_2 = 0$, and ϕ_1 is obtained from the solution of $I(\phi) = I_1(\phi-\phi_1) = I_2(\phi_1)$. Inserting $M^{\sigma}(\phi)$ into Eq. (38), calculating $I^{\rm wl}(\phi) = -2\partial S^{\rm wl}(\phi)/\partial\phi$, and inserting the result into Eq. (39), we obtain the weak localization generating function $g^{\rm wl}(\varepsilon)$, which we expand in powers of ε to get

$$\begin{aligned}
g^{\rm wl}(\varepsilon) = -\frac{(2-\beta)(1+a)aT_2^2T_1^2}{\beta(T_1+aT_2)^3}\Bigg\{1 &+ \frac{1}{(T_1+aT_2)^3}\left[-(3-4T_2)T_1^3 + 2((3-4T_2)-4aT_2)T_2T_1^5\right.\\
&\left. + a^2(3+4aT_2)T_2^2T_1 - 3a^3T_2^3\right]\varepsilon^2 + \frac{1}{(T_1+aT_2)^6}\left[\left(2-(10-9T_2)T_2^2\right)T_1^6\right.\\
&+ a\left(8(2-3a)T_2 - \left(18-49T_2+33T_2^2\right)\right)T_2T_1^5 - a^2\{9+52a-4(4(1+a^2)+17a)T_2\}T_2^3T_1^4\\
&\left. + a^4(16+49a+9a^2T_2)T_2^5T_1^2 - 2a^5(9+5aT_2)T_2^5T_1 - 2a^6T_2^6\right]\varepsilon^4\Bigg\} + \mathcal{O}(\varepsilon^6),
\end{aligned}$$

where $a = N_2/N_1$ is the ratio of the number of open channels in each connector.

Using the above equation one can easily calculate the first three charge transfer cumulants, which for brevity will not be displayed here. The analytical expressions for the first two cumulants are in perfect agreement with the results obtained in Ref. 38. The above equation also coincides, for vanishing Ehrenfest time, with the semiclassical trajectory-based result obtained in Ref. 39. We stress that the result for the third cumulant, which was easily obtained from the σ-model expansion, would require a very cumbersome calculation in the diagrammatic technique.

In the next subsection, we calculate the weak localization corrections to the first three charge transfer cumulants of the homogeneous quantum chain.

B. Homogeneous chain

We start by presenting the eigenvalues of the finite element version of the Cooper propagator, which was obtained using the same procedure described in the previous subsection:

$$M_j^+(\phi) = 4Z(\phi)\left(\cos\frac{\pi j}{N} - 1\right)\left[2Z(\phi)\sin^2\frac{\phi}{N} + \cos\frac{\phi}{N}\right], \tag{43}$$

and

$$M_j^-(\phi) = 4Z(\phi)\left(\cos\frac{\phi}{N} - \cos\frac{\pi j}{N}\right), \tag{44}$$

where $Z(\phi) \equiv T/\{4-4T\sin^2[\phi/(2N)]\}$. Setting $\beta = 1$ and inserting these eigenvalues into Eq. (38), we obtain

$$\begin{aligned}
S^{\rm wl}(\phi) = &\frac{(N-1)}{2}\ln\left(2Z(\phi)\sin^2\frac{\phi}{N} + \cos\frac{\phi}{N}\right)\\
&- \frac{1}{2}\ln\left(\cos\frac{\phi}{N}\right) + \frac{1}{2}\ln\left(\frac{\sin\frac{2\phi}{N}}{\sin\phi}\right).
\end{aligned} \tag{45}$$

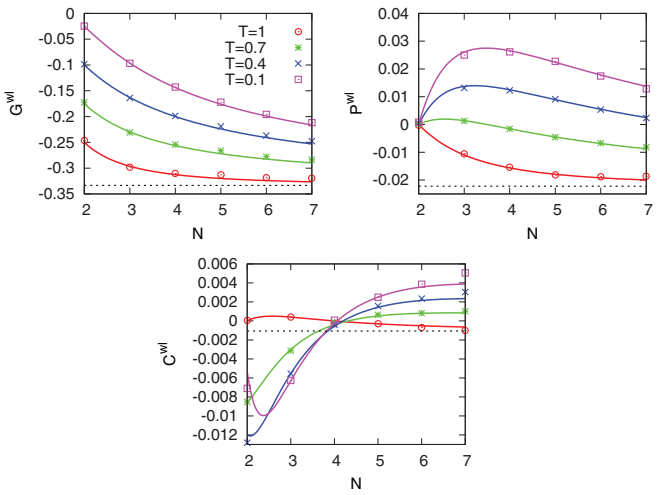

FIG. 5. (Color online) Behavior of the weak localization corrections of transport observables of a quantum chain. The conductance (top left), shot-noise power (top right), and skewness (bottom) are shown as a function of the number of dots in the chain, for $T = 1$ (red line), $T = 0.7$ (green line), $T = 0.4$ (blue line), and $T = 0.1$ (magenta line). The special symbols represent our numerical data for each observable. The quantum wire limits are shown by horizontal lines. The respective values are $-1/3$ for the conductance, $-1/45$ for the shot-noise power, and $-1/945$ for the skewness.

Calculating $I^{\rm wl}(\phi) = -2\partial S^{\rm wl}(\phi)/\partial\phi$ and inserting the result into Eq. (39), we obtain the weak localization generating function $g^{\rm wl}(\varepsilon)$ as an expansion in powers of ε. The weak localization correction for the first three charge transfer cumulants can be obtained by substituting this expansion into Eq. (40). The analytical expressions are given below and the behavior as a function of the number of connectors is shown in Fig. 5. The weak localization correction for the conductance in given by

$$G^{\rm wl} = -\frac{1}{3N^2}\,(N-1)\,(N-2+3T)\,. \tag{46}$$

This result is in complete agreement with what we obtained via a simple extension of the diagrammatic technique for integration over the unitary group. We also checked Eq. (46) with numerical simulations using the random transfer matrix model, Eq. (5), and found very good agreement, as can be seen in Fig. 5. We remark that the above expression reproduces for $T = 1$ the result obtained by Argaman,[40] $g^{\rm wl} = -1/3(1 - 1/N^2)$, using a semiclassical approach. In the limit $T \to 0$, where the system becomes a chain of tunnel junctions, we recover the result obtained in Ref. 19. The results for the weak localization of the shot noise and the third cumulant are given by

$$P^{\rm wl} = -\frac{1}{45N^4}\,(N-1)\,(N-2)\,(N+2)\,(N+15T-14)\,, \tag{47}$$

and

$$C^{\rm wl} = -\frac{1}{945N^6}(N-1)[N^5 - (62-63T)N^4 - 20N^3 + (1240-1260T)N^2 + 64N + 2f(T)]. \tag{48}$$

respectively, where $f(T) \equiv 945T^3 - 2835T^2 + 3906T - 1984$.

Note that for $N \gg 1$ the above expressions for $G^{\rm wl}$ and $P^{\rm wl}$ tend to the values $-1/3$ and $-1/45$ obtained from a random matrix description[41] of a disordered quantum wire. In Fig. 5 we show the behavior of these corrections as a function of the number of connectors in the circuit for several values of the transparency T. We observe that both the second cumulant (top right figure), and the third cumulant (bottom figure) show a nonmonotonous behavior for certain values of T and a striking change of sign at some critical chain size. This change of sign in $P^{\rm wl}$ and $C^{\rm wl}$ is quite unexpected, since there is no breaking of symmetry when we increase the size of the chain. The above expressions also show another nontrivial feature concerning the role of the barriers' transparencies in the ballistic-diffusive crossover in a quantum chain. One could naively imagine that the lower the transparency of the barriers between the quantum dots, the closer an array of quantum dots is from a diffusive wire, since the number of effective scattering events increases. But, as we can see in Fig. 5 this is not what happens. The cases of ideal barriers (red lines) converge to the quantum wire values (dashed lines) much faster than the cases of barriers with low transparencies (e.g., $T = 0.1$, the magenta line) as a function of the number of connectors. We can understand this behavior by observing that the density of Fabry-Perot modes increases with the transparency of the barriers in the homogeneous case, thus pushing the system, as we increase the number of dots in the chain, towards the diffusive regime, where the density of FP modes satisfies the relation $\lim_{N\to\infty} \nu(0)/g = 1$. It would be interesting to find alternative physical explanations for these weak-localization effects using concepts from semiclassical trajectory-based approaches.[39,42] The trajectory-based generating function method presented in Ref. 43 appears to be particularly promising for this purpose.

In the next subsection, we present an analytical expression for the weak localization correction of the conductance in the crossover regime.

C. The crossover regime

In the presence of both an external magnetic field and spin-orbit scattering we have partial breaking of time-reversal symmetry and spin-rotation invariance. These effects can be accounted for by introducing additional terms in the σ-model action. The weak localization corrections of the charge transfer cumulants are sensitive to these new terms, as can be seen from the modification in the generating function, derived in Ref. 19, and shown below:

$$S^{\rm wl}(\phi) = \frac{1}{4}\sum_{j=1}^{N-1}\left[\ln\left(\frac{M_j^-(\phi)+\eta_H}{M_j^+(\phi)+\eta_H}\right) + 3\ln\left(\frac{M_j^+(\phi)+\eta_H+\eta_{\rm SO}}{M_j^-(\phi)+\eta_H+\eta_{\rm SO}}\right)\right], \tag{49}$$

where the parameters η_H and $\eta_{\rm SO}$ are magnetic and spin-orbit scattering rates, which are related to the breaking of time-reversal symmetry and spin-rotation invariance respectively. The pure symmetry ensembles of random matrix theory are obtained by setting $\eta_H = 0$ and $\eta_{\rm SO} = 0$ for the orthogonal

ensemble, also charaterized by Dyson's index $\beta = 1$; $\eta_H \to \infty$ for the unitary ensemble, $\beta = 2$; and $\eta_H = 0$ and $\eta_{SO} \to \infty$ for the symplectic ensemble, $\beta = 4$. Substituting the Cooper propagator eigenvalues of the chain $M_j^{\pm}(\phi)$, Eqs. (43) and (44), into Eq. (49), we can calculate analytical expressions for the weak localization corrections of all cumulants using Eq. (40). The resulting expressions for P^{wl} and C^{wl} are somewhat cumbersome, and thus we shall present only the result for the conductance, which can be written in the following rather neat form:

$$G^{wl} = -\frac{T}{2N^2}\sum_{j=1}^{N-1}\frac{\left(T+(1-T)\cos\frac{\pi j}{N}\right)\left[(2\eta_H-\eta_{SO})+2T\left(1-\cos\frac{\pi j}{N}\right)\right]}{T^2\left(1-\cos\frac{\pi j}{N}\right)^2+\left[\eta_H^2+2\left(T\left(1-\cos\frac{\pi j}{N}\right)+\eta_{SO}\right)\eta_H+T\left(1-\cos\frac{\pi j}{N}\right)\eta_{SO}\right]}. \quad (50)$$

This formula generalizes several previous results of the literature. For instance, if we set $\eta_{SO} = 0$, we obtain

$$G^{wl} = -\frac{T}{N^2}\sum_{j=1}^{N-1}\frac{T+(1-T)\cos\frac{\pi j}{N}}{\eta_H+T\left(1-\cos\frac{\pi j}{N}\right)}, \quad (51)$$

in agreement with Ref. 44. For $N = 3$ (two dots) we obtain

$$G^{wl} = -\frac{2T^2}{9}\frac{3T+1+4\eta_H}{(3T+2\eta_H)(T+2\eta_H)}, \quad (52)$$

which reproduces the result obtained in Ref. 45. In the case of just one quantum dot with nonideal contacts we obtain

$$G^{wl} = -\frac{G_1G_2(G_1T_2+G_2T_1)(G+2\eta_H-\eta_{SO})}{G^2(G+2\eta_H)(G+2\eta_H+2\eta_{SO})}, \quad (53)$$

where, $G = G_1 + G_2$. This result was obtained in Ref. 46 using a diagrammatic technique for integration over the unitary group.

The main crossover effect on the WL correction of the conductance is a change of sign induced by symmetry breaking. The situation is, however, much richer for higher-order cumulants, as can be seen from the single-dot result of Refs. 38 and 46, where the sign of the shot-noise power WL correction can be changed by varying the barriers' transparencies without breaking any symmetry or by breaking TR symmetry with nonideal contacts in the presence of SR invariance. The detailed analysis of crossover effects on the weak-localization correction of higher-order cumulants of the chain would benefit greatly from numerical simulations using the transfer matrix model. Since the inclusion of the symmetry breaking fields in the presence of chaotic scattering requires a substantial extension of our current numerical procedure, we leave this discussion for a future publication.

V. SUMMARY AND CONCLUSIONS

The study of charge, spin, and heat transport through quantum networks is a very active and exciting research field. The existence of a great variety of transport regimes, ranging from ballistic to metallic and insulating behaviors poses serious challenges, both theoretical and experimental, in the development of appropriate tools to describe and control the quantum mechanisms underlying the observed phenomena. In this work, we provide one step forward in this quest by studying in detail the statistics of charge transfer through a chain of chaotic quantum dots in the semiclassical and weak-localization regimes. We observed that the density of transmission eigenvalues, obtained from the semiclassical term of the GF, exhibits a quantum transition, associated with the emergence of Fabry-Perot modes, in a region of the parameter space of barriers' transparencies that expands by increasing the number of quantum dots in the chain. We demonstrated that the presence of these Fabry-Perot modes plays a decisive role in controlling the ballistic-diffusive crossover. It appears to be possible to delay or even suppress the emergence of the universal diffusive behavior by tuning the barrier's transparencies outside the region where the system sustains Fabry-Perot modes. We also found interesting nonmonotonic behaviors in the leading semiclassical terms and changes of sign in the weak-localization corrections of high-order charge transfer cumulants, as a function of the number of dots. Our results agree well with independent analytical calculations using a diagrammatic technique for integration over the unitary group and also with numerical simulations using the transfer matrix model.

There are many ways in which our work could be extended. One interesting possibility is the inclusion of a coupling to an electromagnetic environment, which can be used as an effective model of Coulomb interactions and dephasing.[1] These effects are essential if the temperature dependence of high-order cumulants are to be properly described.[45] The dependence of the weak-localization correction on the topology of the quantum dot network is also an interesting subject for future research, which would have important connections with the literature on disordered quantum networks.[47] Last, but not least, we must mention the recent efforts to understand the Anderson transition in quantum networks. Interesting results using the finite-element version of a modified supersymmetric σ model[48] suggest that there is room for advances in this challenging problem as well.

ACKNOWLEDGMENTS

This work was partially supported by CNPq (Brazilian Agency), FACEPE (Pernambuco State Agency), FAPITEC (Sergipe State Agency), and FAPESP (São Paulo State Agency). G.C.D.F. is thankful to Amir Caldeira for fruitful discussions on the subject in his one-year stay at Universidade Estadual de Campinas (UNICAMP).

[1]For a review, see Yu. V. Nazarov, and Ya. M. Blanter, *Quantum Transport: Introduction to Nanoscience* (Cambridge University Press, Cambridge, UK, 2009).
[2]S. Oberholzer, E. V. Sukhorukov, C. Strunk, C. Schönenberger, T. Heinzel, and M. Holland, Phys. Rev. Lett. **86**, 2114 (2001).
[3]S. Oberholzer, E. V. Sukhorukov, C. Strunk, and C. Schönenberger, Phys. Rev. B **66**, 233304 (2002).
[4]W. Song, A. K. M. Newaz, J. K. Son, and E. E. Mendez, Phys. Rev. Lett. **96**, 126803 (2006).
[5]K. K. Gomes, W. Mar, W. Ko, F. Guinea, and H. C. Manoharan, Nature (London) **483**, 306 (2012).
[6]A. Singha, M. Gibertini, B. Karmakar, S. Yuan, M. Polini, G. Vignale, M. I. Katsnelson, A. Pinczuk, L. N. Pfeiffer, and K. W. West, Science **332**, 1176 (2011).
[7]V. Pellegrini, G. De Simoni, A. Singha, M. Gibertini, B. Karmakar, M. Polini, V. Piazza, L. N. Pfeiffer, K. W. West, and F. Beltram, Appl. Phys. Lett. **97**, 132113 (2010).
[8]Iulia Buluta and Franco Nori, Science **326**, 108 (2009).
[9]T. Byrnes, N. Y. Kim, K. Kusudo, and Y. Yamamoto, Phys. Rev. B **78**, 075320 (2008).
[10]L. S. Levitov, H. Lee, and G. B. Lesovik, J. Math. Phys. **37**, 4845 (1996).
[11]R. J. Glauber, Phys. Rev. **131**, 2766 (1963).
[12]I. Klich and L. S. Levitov, Phys. Rev. Lett. **102**, 100502 (2009).
[13]H. F. Song, S. Rachel, C. Flindt, I. Klich, N. Laflorencie, and K. Le Hur, Phys. Rev. B **85**, 035409 (2012).
[14]M. Esposito, U. Harbola, and S. Mukamel, Rev. Mod. Phys. **81**, 1665 (2009).
[15]T. A. Brun, Phys. Rev. A **61**, 042107 (2000); Am. J. Phys. **70**, 719 (2002).
[16]S. Pilgram, A. N. Jordan, E. V. Sukhorukov, and M. Büttiker, Phys. Rev. Lett. **90**, 206801 (2003).
[17]A. M. S. Macêdo, Phys. Rev. B **69**, 155309 (2004).
[18]C. W. J. Beenakker, Rev. Mod. Phys. **69**, 731 (1997).
[19]G. Campagnano, and Yu. V. Nazarov, Phys. Rev. B **74**, 125307 (2006).
[20]M. J. M. de Jong and C. W. J. Beenakker, Phys. Rev. B **51**, 16867 (1995); Y. M. Blanter and E. V. Sukhorukov, Phys. Rev. Lett. **84**, 1280 (2000).
[21]M. Vanević and W. Belzig, Europhys. Lett. **75**, 604 (2005).
[22]S. Gustavsson, R. Leturcq, B. Simovič, R. Schleser, T. Ihn, P. Studerus, K. Ensslin, D. C. Driscoll, and A. C. Gossard, Phys. Rev. Lett. **96**, 076605 (2006); S. Gustavsson, R. Leturcq, T. Ihn, K. Ensslin, M. Reinwald, and W. Wegscheider, Phys. Rev. B **75**, 075314 (2007).
[23]P. W. Brouwer and C. W. J. Beenakker, J. Math. Phys. **37**, 4904 (1996).
[24]F. A. G. Almeida, S. Rodríguez-Pérez, and A. M. S. Macêdo, Phys. Rev. B **80**, 125320 (2009).
[25]G. C. Duarte-Filho, A. F. Macedo-Junior, and A. M. S. Macêdo, Phys. Rev. B **76**, 075342 (2007).
[26]K. B. Efetov, *Supersymmmetry in Disorder and Chaos* (Cambridge University Press, Cambridge, UK, 1997).
[27]B. Rejaei, Phys. Rev. B **53**, R13235 (1996).
[28]K. Życzkowski and M. Kuś, J. Phys. A **27**, 4235 (1994).
[29]P. A. Mello and N. Kumar, *Quantum Transport in Mesoscopic Systems: Complexity and Statistical Fluctuations* (Oxford University Press, New York, 2004).
[30]Yu. V. Nazarov, and D. A. Bagrets, Phys. Rev. Lett. **88**, 196801 (2002).
[31]Yu. V. Nazarov, in *Quantum Dynamics of Submicron Structures*, edited by H. A. Cerdeira, B. Kramer, and G. Schön, NATO ASI Series, Vol. E291 (Kluwer, Dordrecht, 1995); Yu. V. Nazarov, Superlatt. Microstruct. **25**, 1221 (1999).
[32]A. M. S. Macêdo, Phys. Rev. B **61**, 4453 (2000).
[33]P. Marconcini, M. Macucci, G. Iannaccone, and B. Pellegrini, Phys. Rev. B **79**, 241307R (2009).
[34]A. M. S. Macêdo and A. M. C. Souza, Phys. Rev. E **71**, 066218 (2005).
[35]A. L. R. Barbosa, A. F. Macedo-Junior, and A. M. S. Macêdo, Phys. Rev. B **78**, 045306 (2008).
[36]G. C. Duarte-Filho and A. M. S. Macêdo, Phys. Rev. B **80**, 035311 (2009).
[37]C. W. J. Beenakker and M. Büttiker, Phys. Rev. B **46**, 1889 (1992).
[38]J. G. G. S. Ramos, A. L. R. Barbosa, and A. M. S. Macêdo, Phys. Rev. B **78**, 235305 (2008).
[39]R. S. Whitney, Phys. Rev. B **75**, 235404 (2007).
[40]N. Argaman, Phys. Rev. B **53**, 7035 (1996).
[41]A. M. S. Macêdo and J. T. Chalker, Phys. Rev. B **49**, 4695 (1994).
[42]R. S. Whitney and Ph. Jacquod, Phys. Rev. Lett. **103**, 247002 (2009).
[43]J. Kuipers and K. Richter, J. Phys. A **46**, 055101 (2013).
[44]D. S. Golubev and A. D. Zaikin, Phys. Rev. B **74**, 245329 (2006).
[45]J. N. Kupferschmidt and P. W. Brouwer, Phys. Rev. B **78**, 125313 (2008).
[46]J. G. G. S. Ramos, A. L. R. Barbosa, and A. M. S. Macêdo, Phys. Rev. B **84**, 035453 (2011).
[47]C. Texier, P. Delplace, and G. Montambaux, Phys. Rev. B **80**, 205413 (2009).
[48]M. Disertori, T. Spencer, and M. R. Zirnbauer, Commun. Math. Phys. **300**, 435 (2010).